The Journal of Chemical Physics

Molecular simulation of thermodynamic and transport properties for the H_2O+NaCl system

Cite as: J. Chem. Phys. **141**, 234507 (2014); https://doi.org/10.1063/1.4903928
Submitted: 11 November 2014 • Accepted: 29 November 2014 • Published Online: 18 December 2014

Gustavo A. Orozco, Othonas A. Moultos, Hao Jiang, et al.


View Online

Export Citation

CrossMark

ARTICLES YOU MAY BE INTERESTED IN

A general purpose model for the condensed phases of water: TIP4P/2005
The Journal of Chemical Physics **123**, 234505 (2005); https://doi.org/10.1063/1.2121687

A force field of Li^+, Na^+, K^+, Mg^{2+}, Ca^{2+}, Cl^-, and SO_4^{2-} in aqueous solution based on the TIP4P/2005 water model and scaled charges for the ions
The Journal of Chemical Physics **151**, 134504 (2019); https://doi.org/10.1063/1.5121392

Simulations of activities, solubilities, transport properties, and nucleation rates for aqueous electrolyte solutions
The Journal of Chemical Physics **153**, 010903 (2020); https://doi.org/10.1063/5.0012102

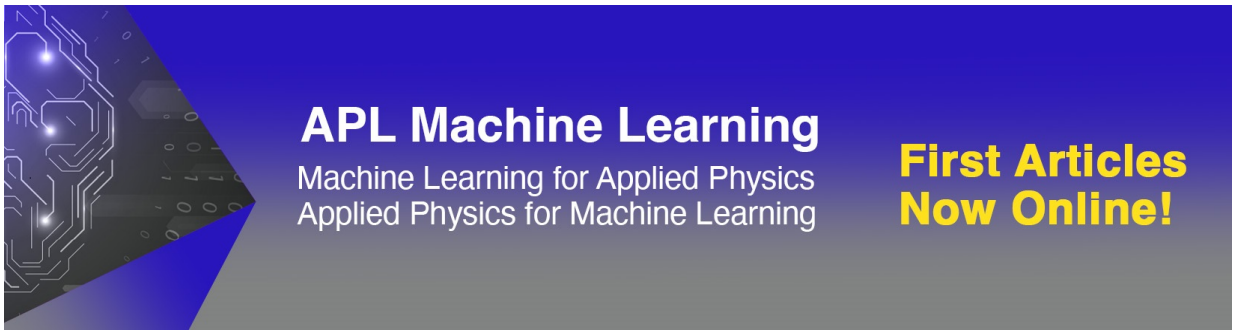

AIP Publishing

© 2014 AIP Publishing LLC.

Molecular simulation of thermodynamic and transport properties for the H_2O+NaCl system

Gustavo A. Orozco,[1] Othonas A. Moultos,[2] Hao Jiang,[1] Ioannis G. Economou,[2] and Athanassios Z. Panagiotopoulos[1,a)]

[1]*Department of Chemical and Biological Engineering, Princeton University, Princeton, New Jersey 08544, USA*

[2]*Chemical Engineering Program, Texas A&M University at Qatar, P.O. Box 23874, Doha, Qatar*

(Received 11 November 2014; accepted 29 November 2014; published online 18 December 2014)

Molecular dynamics and Monte Carlo simulations have been carried out to obtain thermodynamic and transport properties of the binary mixture H_2O+NaCl at temperatures from $T = 298$ to 473 K. In particular, vapor pressures, liquid densities, viscosities, and vapor-liquid interfacial tensions have been obtained as functions of pressure and salt concentration. Several previously proposed fixed-point-charge models that include either Lennard-Jones (LJ) 12-6 or exponential-6 (Exp6) functional forms to describe non-Coulombic interactions were studied. In particular, for water we used the SPC and SPC/E (LJ) models in their rigid forms, a semiflexible version of the SPC/E (LJ) model, and the Errington-Panagiotopoulos Exp6 model; for NaCl, we used the Smith-Dang and Joung-Cheatham (LJ) parameterizations as well as the Tosi-Fumi (Exp6) model. While none of the model combinations are able to reproduce simultaneously all target properties, vapor pressures are well represented using the SPC plus Joung-Cheathem model combination, and all LJ models do well for the liquid density, with the semiflexible SPC/E plus Joung-Cheatham combination being the most accurate. For viscosities, the combination of rigid SPC/E plus Smith-Dang is the best alternative. For interfacial tensions, the combination of the semiflexible SPC/E plus Smith-Dang or Joung-Cheatham gives the best results. Inclusion of water flexibility improves the mixture densities and interfacial tensions, at the cost of larger deviations for the vapor pressures and viscosities. The Exp6 water plus Tosi-Fumi salt model combination was found to perform poorly for most of the properties of interest, in particular being unable to describe the experimental trend for the vapor pressure as a function of salt concentration. © *2014 AIP Publishing LLC*. [http://dx.doi.org/10.1063/1.4903928]

I. INTRODUCTION

The behavior of aqueous electrolyte solutions has been extensively studied in the context of geochemistry, interplanetary science, separation processes, and biophysical chemistry.[1] An accurate estimation of thermodynamic and transport properties of the H_2O+NaCl system is required for the design of new processes in connection to several major current research thrusts. For example, desalination processes are important for parts of the world where fresh water supplies are limited. Aqueous electrolyte thermodynamic and transport properties play a key role in carbon capture and storage processes, in which CO_2 is injected into geologic formations that typically contain aqueous brines.

From a physicochemical point of view, the polar and hydrogen-bonding characteristics of water combined with the ionic character of strong electrolytes make quantitative modeling of solution properties and structure quite challenging. The most common approach for aqueous electrolytes is to use activity coefficient models such as Pitzer's.[2] However, the activity coefficient models cannot be used to obtain volumetric properties. Empirical (cubic) equations of state have been developed for this purpose.[3,4] Although many properties can be correlated with this approach, it is not useful for predictions outside the range of experimental data. Models based on perturbation theory (e.g., statistical associating fluid theory) have been used to study aqueous solutions of electrolytes in recent years. Galindo *et al.* developed such an equation of state to study the vapor pressures and liquid densities of aqueous solutions of strong electrolytes at low temperatures.[5] Weak electrolyte solutions were modeled by Held and Sadowski.[6] Economou *et al.*[7] studied the vapor-liquid equilibria of several associated alkali halide salts at elevated pressures and temperatures using the associated perturbed-anisotropic-chain theory. These models can also be used to predict interfacial properties of electrolyte solutions when combined with density functional theory.[8] In these perturbation theory based models, water is often modeled as a dielectric continuum, and electrostatic interactions are handled approximately through the Poisson-Boltzmann or integral equations, which limits their applicability and predictive power.

Several prior molecular simulation studies have been performed for aqueous electrolyte solutions, in particular for the system H_2O+NaCl of interest to the present work. Many of these studies have focused on the structure of the solution. For instance, Hummer *et al.*[9] carried out molecular dynamics simulations of the effect of salt concentration on the pair

a)Author to whom correspondence should be addressed. Electronic mail: azp@princeton.edu

 © 2014 AIP Publishing LLC

correlation functions, using SPC[10] as the water model and the Pettitt and Rossky parameters[11] to describe ion-ion and water-ion interactions. A comparable study was carried out by Brodholt[12] using SPC/E[13] as the water model and the Smith-Dang (SD) force field for NaCl.[14] The structure of NaCl solutions using TIP4P[15] as the water model was obtained by Gallo *et al.*[16] using the Jensen[17] ion parameters. Chialvo *et al.*[18] performed molecular dynamics simulations to calculate the association and equilibrium constants of the NaCl ion pair at infinite dilution and supercritical conditions, using SPC water, the Tosi-Fumi (TF)[19] potential to represent the ion-ion interactions and three different potentials to account for the ion-water interactions. Lyubartsev and Laaksonen[20] studied the coordination numbers and three-body correlation functions in NaCl solutions using a flexible version of the SPC water model. Solubility calculations of NaCl in aqueous solutions have been recently reported by Moučka *et al.*[21] using seven force fields compatible with the SPC/E[13] water model. Interestingly, none of the force fields were found to be able to reproduce the experimental data quantitatively. A similar study using the Smith-Dang[14] NaCl force field and SPC/E water was carried out by Sanz and Vega.[22] There have also been several studies regarding the determination of surface tension of electrolyte solutions by computer simulations. Bhatt *et al.* calculated the interfacial tensions of NaCl and NaF solutions by molecular dynamics simulations, and compared explicit-water with solvent-primitive models.[23] Bahadur *et al.* obtained surface tensions for the vapor-liquid, solid-liquid, and solid-vapor interfaces of the NaCl-water-air system.[24] Several polarizable water and ion models have been developed for aqueous salt solutions, most focusing on the structure and thermodynamic properties of dilute solutions.[25–27] Neyt *et al.*[28] obtained the interfacial tension and densities of salt solutions using polarizable water models based on the Drude model; their study concluded that these models are unable to reproduce the changes in surface tension with salt concentration.

Despite the importance of aqueous brines, little prior simulation work has been performed on vapor-liquid equilibria for the system H_2O+NaCl. To the best of our knowledge, the only such prior study is by Strauch and Cummings,[29,30] using Gibbs ensemble Monte Carlo at $T = 375$ and 473 K and a single salt concentration, with SPC water and the Tosi-Fumi model for ion-ion interactions. Water-ion interactions were calculated using the parameters of Chandrasekhar *et al.*[31] This early study did not reach quantitative conclusions on the effects of salt on the vapor pressure of water. The only prior study of the viscosity for the binary system H_2O+NaCl is by Ge *et al.*[32] who used non-equilibrium molecular dynamics simulations at supercritical conditions for the solvent.

The present work aims to study several key properties of the mixture H_2O + NaCl over a wide range of salt concentrations, temperatures, and pressures, using different fixed-point-charge force field combinations. The objective of the study is to validate such model combinations with respect to vapor pressures (and by implication osmotic coefficients), liquid densities, vapor-liquid interfacial tensions, and viscosities of the mixture. The NaCl force fields we consider are compatible with the SPC[10] and the SPC/E[13] water models. In addition, a semiflexible version of the SPC/E water model[33] is of interest. Recent work of Orozco *et al.*[34] found that the Errington-Panagiotopoulos Exp6 water model[35] is able to reproduce accurately the phase behavior of the mixture $H_2O + CO_2$ over a wide range of pressures and temperatures; for this reason this model is also included here. For the NaCl Lennard Jones (LJ)-based force fields, the SD[14] and Joung-Cheatham (JC)[36] models are considered since these reproduce the solubilities of NaCl in water reasonably well, according to prior studies.[21,22] To combine with the Exp6 water model, the TF potential[19] for NaCl is used, as it has a similar functional form and reproduces with good accuracy physical properties of pure NaCl, such as the melting point.[37]

This paper is organized as follows. Simulation details and methodology of the Monte Carlo and Molecular Dynamics calculations are given in Secs. II A and II B, respectively. The force field parameters are described in Sec. II C. Results for vapor pressures, liquid densities, viscosities, and interfacial tensions are presented in Sec. III. Finally, the main conclusions and prospects are given in Sec. IV.

II. METHODS

A. Monte Carlo

Gibbs-ensemble Monte Carlo simulations were performed at constant volume and temperature (NVT)[38,39] so as to obtain the vapor pressures of the binary system. Liquid densities were calculated in the isothermal-isobaric (NPT) ensemble. In addition to in-house developed code, the Cassandra suite of Monte Carlo codes[40] (customized beta release version) were used for the calculations, with excellent agreement between the two sets of codes.

For both the Gibbs- and NPT-ensemble simulations, a total of 550 water molecules along with 1–54 NaCl molecules were used in most of the runs. The lowest number of NaCl molecules corresponds to molality $m = 0.10$ mol/kg and the highest number corresponds to $m = 5.45$ mol/kg. Finite-size effects were tested by doubling the system size at both low and high molalities at a single temperature, $T = 473$ K; the results obtained were within statistical uncertainties of those of the base system size, suggesting that finite-size effects are small. A typical simulation run consisted of 50×10^6 Monte Carlo steps for equilibration, followed by a production period of 150×10^6 Monte Carlo steps. Depending on the number of salt molecules, this took between 40 and 50 h using four 2.6 GHz Sandybridge processors. Statistical uncertainties were obtained by dividing the production period of the simulations into four blocks.

For the LJ potential, a cutoff of 9 Å was used and analytical long-range corrections were applied. The Ewald summation was used to handle long-range electrostatic interactions with a maximum of 7 vectors for each direction in reciprocal space. The Monte Carlo moves used for the Gibbs ensemble simulations were volume changes (constituting a fraction of 0.005 of total moves), rigid rotations (0.325), center of mass translations (0.325), and transfer of particles with configurational bias (0.345).[41] It was assumed that no salt is present

in the vapor phase, and the transfer probability of NaCl was set to zero, as in Ref. 29. This is not an artificial constraint; molecular dynamics simulations at comparable conditions[42] demonstrate that there is no salt present in the vapor phase at the temperature range of interest, even when ions are allowed – in principle – to move between phases. For the *NPT* calculations, the Monte Carlo moves used were isotropic volume changes (0.005), and rigid rotations or center-of-mass translations in equal proportions.

B. Molecular dynamics

Molecular dynamics simulations for the viscosity were performed in cubic boxes with periodic boundary conditions imposed in all directions, using the open-source GROMACS package[43–45] (Version 4.6.3). Initially, the system was equilibrated for a period of 10 ns in the isothermal-isobaric (*NPT*) ensemble, using a Berendsen thermostat and barostat,[46] with both coupling constants set to 1 ps. This period was more than adequate for the system structure and thermodynamic properties to converge and ensured well-equilibrated systems at all temperatures and pressures studied. The presence of strong ionic interactions necessitates the use of longer equilibration periods relative to simulations of pure water. Subsequently, for the determination of viscosities, 10 ns production runs were performed in the canonical (NVT) ensemble, with integration timestep of 1 fs. The temperature was maintained using the Nosé-Hoover thermostat,[47,48] with coupling constant of 1 ps. The elements of the pressure tensor were sampled every timestep. As previously, the number of H_2O molecules was 500 while the number of NaCl molecules varied according to the desired molality. Long-range Coulombic interactions were handled using the particle-mesh Ewald method.[49,50] Fourth-order interpolation was used along with a Fourier-spacing parameter of 0.12, corresponding to an accuracy of approximately 5×10^{-3} in electrostatic energy. The cutoff distance was set to 11 Å, both for the LJ interactions and real-space electrostatics. Each run required about 5 wall-clock hours to be completed, using 32 cores of Intel Xeon 2.7 GHz processors. For the calculation of shear viscosity the Green-Kubo relations[51,52] were used,

$$\eta(t) = \frac{V}{k_B T}\int_0^t \langle P_{\alpha\beta}(t_0) P_{\alpha\beta}(t_0+t)\rangle dt, \qquad (1)$$

where V is the volume of the simulation box and $P_{\alpha\beta}$ denotes the off-diagonal element of the pressure tensor. The angle brackets indicate an ensemble average over all time origins t_0. In order to improve statistics, we averaged the autocorrelation functions over all independent off-diagonal tensor elements[53,54] P_{xy}, P_{xz}, P_{yz}; because of rotational invariance we also added the equivalent $(P_{xx} - P_{yy})/2$ and $(P_{yy} - P_{zz})/2$ terms.[55,56] Viscosity at each state point and the associated statistical uncertainty was calculated from seven independent simulations, each starting from a different initial configuration.

The vapor-liquid interfacial tensions were obtained by interfacial molecular dynamics simulations using LAMMPS[57] (5 September 2014 version). The computation scheme was similar to that used for the determination of viscosities, with simulations performed in the canonical (constant-NVT) ensemble using the Nosé-Hoover thermostat.[47,48] Each run needed about 25 wall-clock hours to be completed when executed on 32 cores. Since the computation time for the direct interfacial simulations was longer, interfacial tensions were calculated from a single simulation per state point, and statistical uncertainties were obtained from block averages. The interfacial tension was evaluated as in a prior study,[42] using the diagonal stress tensor elements (P_{xx}, P_{yy}, and P_{zz}) through the equation

$$\gamma = \frac{L_z}{2}[\langle P_{zz}\rangle - 0.5\times(\langle P_{xx}\rangle + \langle P_{yy}\rangle)], \qquad (2)$$

where L_z is the longest dimension of the simulation box. The vapor-liquid interface forms along the xy plane. In simulations of inhomogeneous systems, truncation of the Lennard-Jones or Buckingham Exp6 potential at a finite cutoff distance leads to incorrect estimation of interfacial properties.[58] In the present work, instead of using an analytical tail correction, we followed the approach of Veld *et al.*[59] and applied the Ewald summation method to the attractive part of the Lennard-Jones and the Buckingham Exp6 potential. It was found that the interfacial tensions were not sensitive to the cutoff distance when using this approach. Electrostatic interactions were handled by the particle-mesh Ewald summation method as indicated previously.

C. Force field parameters

Tables I and II summarize the force field parameters for the LJ and the Exp6 functional forms which are represented by Eqs. (3) and (4), respectively. As mentioned earlier, for the case of water, the SPC[10] and SPC/E[13] models were considered in their original rigid formulations. Additionally, a semi-flexible SPC/E model[33] and an Exp6 model[35] were also considered. These models are represented by three interactions sites and three partial charges. For the SD[14] and JC[36] models of NaCl, each ion is represented by one LJ site and one point charge located at the center of the ion. The TF model[19] for NaCl was originally expressed as a Buckingham potential. In the original formulation, an additional term proportional to r^{-8} was present, however, for the present study this term was neglected since it does not have a significant effect on the

TABLE I. LJ force field parameters for H_2O and NaCl.

Model	Atom	σ (Å)	ε/k_B (K)	q (e)	Geometry
SPC/E	O	3.166	78.197	−0.8476	$r_{OH} = 1.0$ Å
	H	…	…	+0.4238	$\theta_{H\text{–}O\text{–}H} = 109.5°$
Semiflex.	O	3.166	78.197	−0.8476	$r_{OH} = 1.0$ Å
SPC/E	H	…	…	+0.4238	$\theta_{H\text{–}O\text{–}H} = 109.5°$
					$k_\theta = 46\,067.5$ K/rad^2
SD	Na^+	2.35	65.42	1.0	…
	Cl^-	4.40	50.32	−1.0	…
JC	Na^+	2.16	177.4	1.0	…
	Cl^-	4.831	6.434	−1.0	…

calculated properties. Thus, the final mathematical expression is given by Eq. (5). It is straightforward to see that Eqs. (4) and (5) are related by the expressions given in Eq. (6), which allow the determination of values for $\{\varepsilon_{ij}, r_{ij}^{\min}, \alpha_{ij}\}$ for a given set of Buckingham parameters $\{A_{ij}, B_{ij}, C_{ij}\}$, such as the TF potential for NaCl

$$U^{\mathrm{LJ}}(r_{ij}) = 4\varepsilon_{ij}\left[\left(\frac{\sigma_{ij}}{r_{ij}}\right)^{12} - \left(\frac{\sigma_{ij}}{r_{ij}}\right)^{6}\right], \tag{3}$$

$$U^{\mathrm{Exp6}}(r_{ij}) = \begin{cases} \dfrac{6\varepsilon_{ij}}{\alpha_{ij}-6}\exp\left[\alpha_{ij}\left(1-\dfrac{r_{ij}}{r_{ij}^{\min}}\right)\right] - \dfrac{\alpha_{ij}\varepsilon_{ij}}{\alpha_{ij}-6}\left(\dfrac{r_{ij}^{\min}}{r_{ij}}\right)^{6}; r_{ij} > r_{ij}^{\mathrm{core}}, \\ \infty; r_{ij} < r_{ij}^{\mathrm{core}} \end{cases} \tag{4}$$

$$U^{\mathrm{Buck}}(r_{ij}) = Ae^{-Br_{ij}} - \frac{C}{r_{ij}^{6}}, \tag{5}$$

$$A_{ij} = \frac{6\varepsilon_{ij}e^{\alpha_{ij}}}{\alpha_{ij}-6}; \qquad B_{ij} = \frac{\alpha_{ij}}{r_{ij}^{\min}}; \qquad C_{ij} = \frac{\left(r_{ij}^{\min}\right)^{6}\alpha_{ij}\varepsilon_{ij}}{\alpha_{ij}-6}. \tag{6}$$

The values of σ_{ij} are directly calculated as the distances at which the corresponding potential is equal to zero using Eq. (4). Table II shows the TF numerical values expressed in terms of the Exp6 parameters obtained after following this procedure. For the Exp6 parameters in Table II, we list the values of σ instead of $r^{\min}$ for consistency with the Lennard-Jones potential. In addition, a cutoff distance r^{core} is present in the Exp6 potential of water (Eq. (4)), and its value can be found elsewhere.[35] For Monte Carlo simulations, configurations with oxygen-oxygen intermolecule distance smaller than r^{core} are rejected, while such configurations are never sampled in molecular dynamics simulations.

For both LJ and the Exp6 functional forms, the conventional Lorentz-Berthelot combining rules were used to calculate the unlike-pair interactions for ε_{ij} and σ_{ij}. These rules consist of a geometric-mean combination for ε_{ij} and an arithmetic-mean combination for σ_{ij}, as shown in Eq. (7). The Exp6 models require two additional relations given by Eq. (8)

$$\sigma_{ij} = \frac{\sigma_{ii}+\sigma_{jj}}{2}; \qquad \varepsilon_{ij} = \sqrt{\varepsilon_{ii}\varepsilon_{jj}}, \tag{7}$$

$$r_{ij}^{\min} = \frac{r_{ii}^{\min}+r_{jj}^{\min}}{2}; \qquad \alpha_{ij} = \sqrt{\alpha_{ii}\alpha_{jj}}. \tag{8}$$

For the SD and JC force fields, the LJ σ values are of the same order of magnitude, with Cl^- being larger, as expected from the van der Waals radii of the isolated ions.[60] Nevertheless, the numerical values of ε for ions in the SD model are quite different from the JC model, e.g., the Cl^- energy parameter of the SD force field is almost 10 times higher than the JC one. For the case of the TF model, the σ value for Na^+ is bigger than the one for Cl^-, while the energy parameter ε of Na^+ is almost zero; the values of σ and ε control the softness of the repulsion at short distances, with a small ε making it easier for counterions to approach. At longer distances, the intermolecular interactions are dominated by the Coulombic part of the potential, rather than the LJ or Exp6 part.

TABLE II. Exp6 force field parameters for H_2O and NaCl. Geometry of Exp6 water model: $r_{OH} = 1.0668$ Å, $\theta_{H\text{–}O\text{-}\,\text{–}\,H} = 109.5°$.

Model	Atom	σ (Å)	ε/k_B (K)	α	q (e)
Exp6	O	3.195	159.78	12	− 0.7374
	H	...	...	...	+0.3687
TF	Na^+	5.468	0.276	17.24	1.0
	Cl^-	4.212	83.14	13.29	− 1.0

III. RESULTS

The vapor pressures, liquid densities, viscosities, and interfacial tensions were obtained using the force field models given in Sec. II. Numerical data and simulation uncertainties are listed in the supplementary material.[61] Simulation data extend to concentrations above the experimental solubility of NaCl in water at the corresponding temperatures and pressures. For many of the models studied, model solubilities are actually lower than the experimental ones.[62] However, crystal nucleation in simulations of supersaturated solutions is extremely difficult, as it has to occur by a homogeneous mechanism in a small system. We have confirmed that for all models and concentrations studied the simulation runs were at homogeneous solution conditions, by calculating the pair correlation functions between positive and negative ions (shown as figures in the supplementary material[61]), and by following the time evolution of configurations to ensure that no large ionic aggregates are present.

A. Vapor pressures

Figure 1 shows the vapor pressures as a function of the NaCl concentration in molal units (mol NaCl/kg of H_2O) at two temperatures, $T = 373$ K on the left side and $T = 473$ K

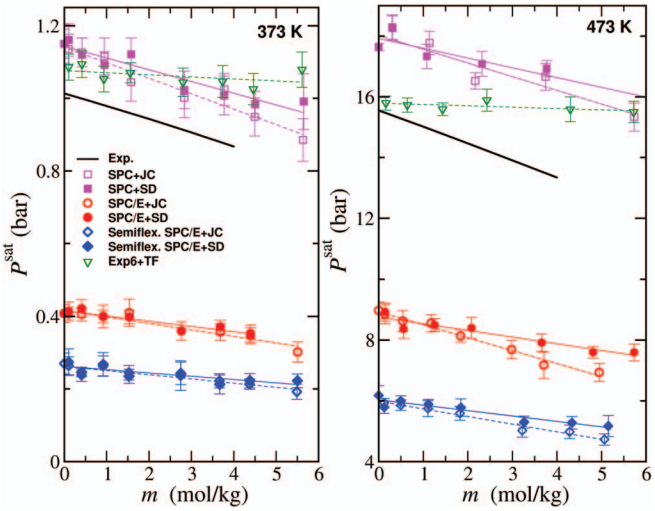

FIG. 1. Vapor pressures, P^{sat} (bar), for the system H_2O + NaCl at $T = 373$ K (left) and $T = 473$ K (right), *versus* molality m (mol NaCl/kg H_2O). Solid black lines are experimental data from Ref. 63. Magenta open and filled squares are for SPC water combined with JC and SD salt models, respectively. Red open and filled circles are for SPC/E combined with JC and SD, respectively. Blue open and filled diamonds are for the semiflexible SPC/E with JC and SD, respectively. Green triangles are for the Exp6 plus TF model. Colored lines through the points are linear least-square fits to the corresponding data sets.

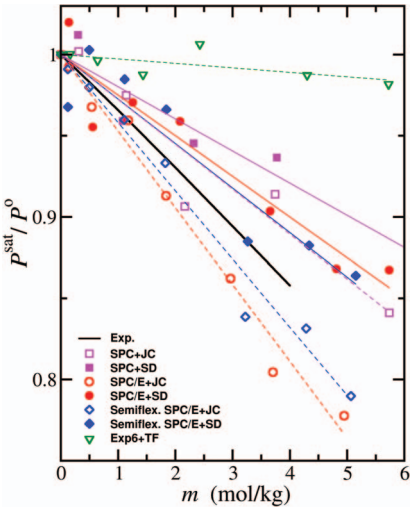

FIG. 2. Vapor pressure ratios, P^{sat}/P^0 for the system H_2O + NaCl at $T = 473$ K *versus* molality m (mol NaCl/kg H_2O). Symbols and lines are as in Figure 1.

on the right side. The vapor pressures at $T = 298$ K were also obtained for several model combinations. However, the calculated vapor pressures at 298 K have larger relative statistical uncertainties because their absolute values are low; results at 298 K are not shown in Figure 1, but given in the supplementary material.[61]

The LJ combinations with the older SPC model best describe the experimental data for the vapor pressures, primarily because the SPC model is close to the vapor pressure of pure water at this temperature. The two salt models, JC and SD, give comparable results, mostly within their respective error bars, but with a slight overall systematic advantage for the SPC+JC model. The combinations that use SPC/E as the water model underpredict the vapor pressures of the mixture by a factor of a little over two. Despite the fact that inclusion of flexibility improves the surface tension and liquid densities of pure water,[33] for the vapor pressure we find that flexibility makes the predictions worse relative to the rigid SPC or SPC/E models. Similar results are found with the semiflexible SPC/E model using the SD ion model. For the Exp6 + TF model combination, the pure component vapor pressure is well represented, so the results start from the correct limit at $m = 0$, but the mixture vapor pressure remains almost constant as the salt concentration increases. In a separate study,[62] this model combination was also found to be poor for the salt activity coefficients in the water phase at $T = 298$ K. A possible reason for these failures may be the inadequate representation of the structure of pure liquid water for the Exp6 model.[35] Another possible reason may be that the TF model that was parameterized for the solid, rather than the aqueous, environment.

The effect of the differences in predictions of the pure component vapor pressures can be eliminated by replotting the data of Figure 1 as the ratio of the vapor pressure at a given molality, P^{sat}, over the vapor pressure of the pure component for the corresponding model, P^0, at $m = 0$. Results for $T = 473$ K are shown in Figure 2, in which the error bars have been omitted for clarity; similar results were obtained at $T = 373$ K. This ratio coincides at low pressures with the activity of the solvent, and is in turn related to the osmotic coefficient of the solution. Figure 2 shows that the semiflexible SPC/E+JC model is the one closest to the experimental data, slightly underpredicting the ratio P^{sat}/P^0 at all concentrations. The semiflexible SPC/E+SD combination is almost as good as the semiflexible SPC/E+JC, with deviations in the opposite direction, slightly overpredicting P^{sat}/P^0. The same trend, overprediction of the ratio P^{sat}/P^0 for the SD salt model and underprediction for the JC model is seen for the SPC/E water model. The exp6+TF model combination is totally inadequate, predicting a much lower slope for P^{sat}/P^0 *versus* salt molality m relative to the experimental data and the other model combinations.

B. Densities

Figure 3 shows the liquid densities of the mixture at $T = 298$, 373, and 473 K, for a subset of the models of Figure 1. Two different pressures were studied, $P = 100$ and 1000 bars, shown on the left and right side, respectively. All model combinations follow the experimental trend, i.e., the mixture density increases as a function of the molality. In general, predicted densities are in reasonable agreement with the experimental data,[63] although the Exp6 + TF combination significantly underestimates the densities at 473 K. The best density predictions are given by the semiflexible SPC/E water with the JC ion model. The inclusion of flexibility improves the densities of the mixtures but has a negative impact on the vapor pressure predictions, as seen earlier. Contrary to the vapor pressure case, where the differences between the SD and JC ion models were small, for the liquid density predictions the differences become more significant at high molalities; the

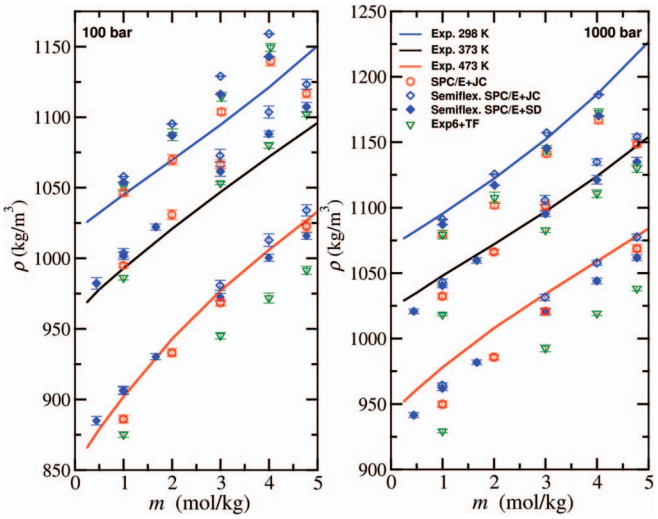

FIG. 3. Liquid densities ρ (kg/m^3) *versus* molality m (mol NaCl/kg H_2O) at $T = 298$, 373, and 473 K. Left and right figures correspond to $P = 100$ and 1000 bars, respectively. Solid lines are experimental data taken from Ref. 63. Symbols are as in Figure 1.

SD salt model better represents the effect of salt on the density at $P = 100$ bars at all three temperatures studied. The SPC model was not included for this part of the study since it is known that it does not reproduce accurately the liquid density of pure water.

C. Viscosities

Figure 4 shows the viscosities at $T = 373$ and 473 K as a function of salt concentration. Simulations were performed at constant pressures of $P = 2$ and $P = 20$ bars, slightly higher than the vapor pressures at the corresponding temperatures. The experimental data correspond to vapor-liquid equilibrium conditions (pressure varies with composition as shown in Figure 1), but at these temperatures the effects of pressure on viscosity are negligible compared to simulation uncertainties, for small pressure differences. Five different models were considered, namely, the rigid and semiflexible SPC/E with JC and SD, and the Exp6+TF combination. The SPC water model was not studied because it does not give good predictions of viscosities of the pure fluid.

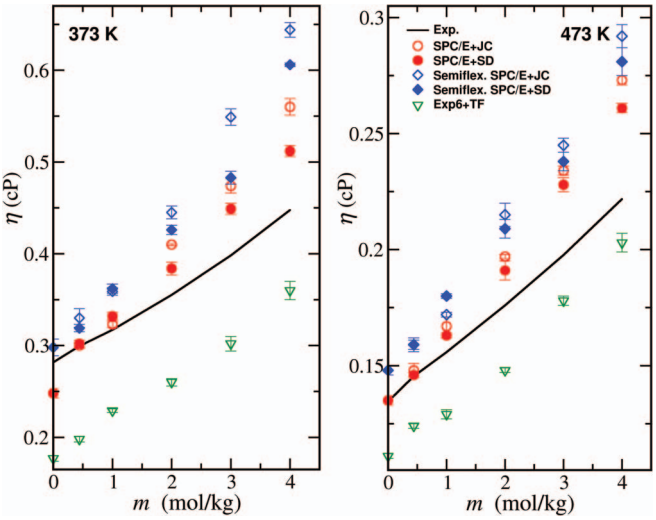

FIG. 4. Viscosities η (cP) *versus* molality m (mol NaCl/kg H_2O) at $T = 373$ K on the left side and $T = 473$ K on the right side. Black solid lines correspond to experimental data.[63] Symbols are as in Figure 1. Simulations were performed at constant pressures of $P = 2$ bars and $P = 20$ bars, respectively, while the experimental data correspond to vapor-liquid equilibrium conditions at the corresponding temperature and composition.

As shown here, the viscosity increases with salt concentration, in qualitative agreement with the experimental trend. The rate of increase is higher than the experimental slope for all models, with the exception of exp6+TF. Thus, for all the LJ combinations, the viscosity predictions are in better agreement with experimental data at low molalities than at high molalities. Predictions using the SPC/E rigid model with the JC ion model are higher than for the SD ion model, so the combination SPC/E+SD produces the best results for the conditions studied. Similar to the vapor pressure case, inclusion of flexibility on the SPC/E water model has an adverse effect on the predictions, producing viscosities which at high molalities are overestimated by a factor of two with respect to the experimental values. Finally, in contrast to the LJ results, the Exp6+TF model underpredicts the viscosities for all the conditions studied.

D. Vapor-liquid interfacial tensions

Figure 5 shows the simulation predictions for the vapor-liquid interfacial tension as function of salt concentration at $T = 298$, 373, and 473 K. Four different force field model combinations were considered: the rigid SPC/E model with SD and JC, and the semiflexible version of the SPC/E model with SD and JC. The SPC model was not investigated in this part, since it significantly underestimates the surface tension of pure water. Additionally, the Exp6 with TF model was also not studied here, due to its unrealistic behavior for the vapor pressure shown in Figure 1.

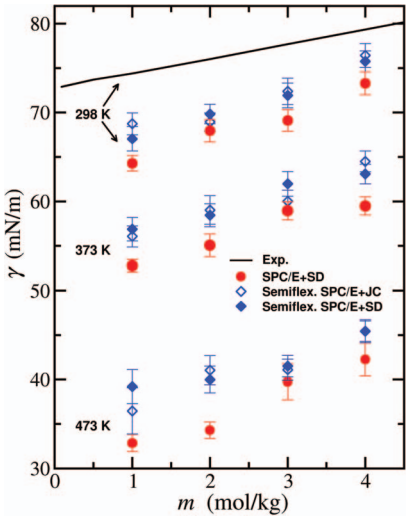

FIG. 5. Vapor-liquid interfacial tensions γ in mN/m *versus* molality m in mol NaCl/kg H_2O at $T = 298$, 373, and 473 K. Black continuous line corresponds to experimental data at $T = 298$ K.[64] Symbols are as in Figure 1.

From the results of Figure 5, the interfacial tensions are seen to increase with salt concentration, in agreement with the experimental trend.[64] All model combinations underestimate the interfacial tension at 298 K at all concentrations (including the pure fluid). A similar underestimation can be expected at 373 K and 473 K, even though experimental data for γ are not available at the higher temperatures as a function of salt content; pure water has γ equal to 58.9 and 37.7 mN/m, respectively. The semiflexible version of the SPC/E water model gives a better value for the interfacial tension relative to the rigid SPC/E water model, which indicates that inclusion of flexibility in the SPC/E water model has a favorable effect for the estimation of interfacial properties. The interfacial tensions predicted from the semiflexible SPC/E with the SD ion model are similar to those obtained from the semiflexible SPC/E with the JC ion model. When combined with the rigid SPC/E water model, JC and SD models also yield similar interfacial tensions. Because of this, the interfacial tensions calculated from the rigid SPC/E with the JC ion model are given in the supplementary material[61] and not shown in Figure 5.

IV. CONCLUSIONS

An extensive study involving several force field combinations was carried out in order to determine the best alternatives for molecular-simulation based description of vapor pressures, liquid densities, viscosities, and vapor-liquid interfacial data for the H_2O + NaCl mixture. Although it was found that none of the studied combinations are able to describe simultaneously all the properties of interest, some models give a good quantitative description of individual properties. The best combinations can be summarized as follows: (i) SPC water plus JC ion model for vapor pressures, (ii) semiflexible SPC/E+JC for liquid densities, (iii) SPC/E+SD for viscosities, and (iv) semiflexible SPC/E+SD or JC for the interfacial tensions. Inclusion of flexibility decreases vapor pressures and increases viscosities with respect to the rigid models. For that reason, despite the fact that using the semiflexible model gives good accuracy for density estimations in general, it is probably not a good alternative; the SPC/E model in its rigid version with the JC ion model is likely to be a better option. The Exp6+TF model combination was found to be inaccurate, as it cannot reproduce the trends on the mixture vapor pressure as a function of molality even qualitatively.

In recent work, our group has studied the behavior of the binary mixture $H_2O + CO_2$ at several conditions of pressures and temperatures characteristic of the carbon sequestration process.[34] It was found that the Exp6 potentials can reproduce accurately the mutual solubilities of the system using non-Lorentz-Berthelot combining rules between unlike molecules. The ternary system $CO_2 + H_2O$ + NaCl is of clear relevance for geochemical storage applications. Given the conclusions of the present study, new Exp6 models for NaCl compatible with the Errington-Panagiotopoulos water model will need to be developed in order to obtain a good description of the ternary system. Studies of such models will also shed light on the underlying reasons for the inaccurate predictions discussed in Sec. III A. Alternatively, polarizable salt and water models can be explored to obtain the properties over broad ranges of temperature and density.

ACKNOWLEDGMENTS

This publication was made possible by NPRP Grant No. 6-1157-2-471 from the Qatar National Research Fund (a member of Qatar Foundation). The statements made herein are solely the responsibility of the authors. Additional support was provided by the Office of Basic Energy Sciences, (U.S.) Department of Energy (DOE), under Award No. DE-SC0002128.

[1] W. Voigt, Pure Appl. Chem. **83**, 1015–1030 (2011).
[2] K. S. Pitzer, J. Phys. Chem. **77**, 268–277 (1973).
[3] A. Haghtalab and S. H. Mazloumi, Fluid Phase Equilib. **285**, 96–104 (2009).
[4] Y. Lin, K. Thomsen, and J. Hemptinne, AIChE J. **53**, 989–1005 (2007).
[5] A. Galindo, A. Gil-Villegas, G. Jackson, and A. N. Burgess, J. Phys. Chem. B **103**, 10272–10281 (1999).
[6] C. Held and G. Sadowski, Fluid Phase Equilib. **279**, 141–148 (2009).
[7] I. G. Economou, C. J. Peters, and J. de Swaan Arons, J. Phys. Chem. **99**, 6182–6193 (1995).
[8] M. Oliveira, F. Llovell, J. Coutinho, and L. F. Vega, J. Phys. Chem. B **116**, 9089–9100 (2012).
[9] G. Hummer, D. M. Soumpasis, and M. Neumann, J. Phys. Condens. Matter **6**, A141–A144 (1994).
[10] H. J. C. Berendsen, J. P. M. Postma, W. F. van Gunsteren, and J. Hermans, Intermol. Forces **14**, 331–342 (1981).
[11] B. M. Pettitt and P. J. Rossky, J. Chem. Phys. **84**, 5836–5842 (1986).
[12] J. Brodholt, Chem. Geol. **151**, 11–19 (1998).
[13] H. J. C. Berendsen, J. R. Grigera, and T. P. Straatsma, J. Phys. Chem. **91**, 6269–6271 (1987).
[14] D. E. Smith and L. X. Dang, J. Chem. Phys. **100**, 3757–3766 (1994).
[15] W. L. Jorgensen, J. Chandrasekhar, J. D. Madura, R. W. Impey, and M. L. Klein, J. Chem. Phys. **79**, 926–935 (1983).
[16] P. Gallo, D. Corradini, and M. Rovere, Phys. Chem. Chem. Phys. **13**, 19814–19822 (2011).
[17] K. P. Jensen and W. L. Jorgensen, J. Chem. Theory Comput. **2**, 1499–1504 (2006).
[18] A. A. Chialvo, P. T. Cummings, H. D. Cochran, J. M. Simonson, and R. E. Mesmer, J. Chem. Phys. **103**, 9379–9387 (1995).
[19] F. G. Fumi and P. Tosi, J. Phys. Chem. Solids **25**, 31–43 (1964).
[20] A. P. Lyubartsev and A. Laaksonen, J. Phys. Chem. **100**, 16410–16418 (1996).
[21] F. Moučka, I. Nezbeda, and W. R. Smith, J. Chem. Phys. **138**, 154102 (2013).
[22] E. Sanz and C. Vega, J. Chem. Phys. **126**, 014507–014513 (2007).
[23] D. Bhatt, J. Newman, and C. J. Radke, J. Phys. Chem. B **108**, 9077–9084 (2004).
[24] R. Bahadur, L. M. Russell, and S. Alavi, J. Phys. Chem. B **111**, 11989–11996 (2007).
[25] P. Kiss and A. Baranyai, J. Chem. Phys. **138**, 204507 (2013).
[26] H. Yu, T. W. Whitfield, E. Harder, G. Lamoureux, I. Vorobyov, V. M. Anisimov, A. D. MacKerell, and B. Roux, J. Chem. Theory Comput. **6**, 774–786 (2010).
[27] S. Tazi, J. J. Molina, B. Rotenberg, P. Turq, R. Vuilleumier, and M. Salanne, J. Chem. Phys. **136**, 114507 (2012).
[28] J. C. Neyt, A. Wender, V. Lachet, A. Ghoufi, and P. Malfreyt, Phys. Chem. Chem. Phys. **15**, 11679–11690 (2013).
[29] H. J. Strauch and P. T. Cummings, Fluid Phase Equilib. **86**, 147–172 (1993).
[30] H. J. Strauch and P. T. Cummings, Fluid Phase Equilib. **83**, 213–222 (1993).
[31] J. Chandrasekhar, D. C. Spellmeyer, and W. L. Jorgensen, J. Am. Chem. Soc. **106**, 903–910 (1984).
[32] S. Ge, X. X. Zhang, and M. Chen, J. Chem. Eng. Data **56**, 1299–1304 (2011).
[33] J. López-Lemus, G. Chapela, and J. Alejandre, J. Chem. Phys. **128**, 174703 (2008).
[34] G. A. Orozco, I. G. Economou, and A. Z. Panagiotopoulos, J. Phys. Chem. B **118**, 11504–11511 (2014).

[35]J. R. Errington and A. Z. Panagiotopoulos, J. Phys. Chem. B **102**, 7470–7475 (1998).
[36]I. S. Joung and T. E. Cheatham, J. Phys. Chem. B **112**, 9020–9041 (2008).
[37]J. Anwar, D. Frenkel, and M. G. Noro, J. Chem. Phys. **118**, 728–735 (2003).
[38]A. Z. Panagiotopoulos, Mol. Phys. **61**, 813–826 (1987).
[39]A. Z. Panagiotopoulos, N. Quirke, M. Stapleton, and D. J. Tildesley, Mol. Phys. **63**, 527–545 (1988).
[40]Cassandra is an open-source code developed in the group of Professor Ed Maginn at the University of Notre Dame and is available from http://www3.nd.edu/~ed/research/cassandra.html.
[41]I. J. Siepmann, Mol. Phys. **70**, 1145–1158 (1990).
[42]Y. Liu, T. Lafitte, A. Z. Panagiotopoulos, and P. G. Debenedetti, AIChE J. **59**, 3514–3522 (2013).
[43]H. J. C. Berendsen, D. van der Spoel, and R. van Drunen, Comput. Phys. Commun. **91**, 43–56 (1995).
[44]E. Lindahl, B. Hess, and D. van der Spoel, J. Mol. Model. **7**, 306–317 (2001).
[45]B. Hess, C. Kutzner, D. van der Spoel, and E. Lindahl, J. Chem. Theory Comput. **4**, 435–447 (2008).
[46]H. J. C. Berendsen, J. P. M. Postma, W. F. van Gunsteren, A. Dinola, and J. R. Haak, J. Chem. Phys. **81**, 3684–3690 (1984).
[47]S. Nosé, Mol. Phys. **52**, 255–268 (1984).
[48]W. G. Hoover, Phys. Rev. A **31**, 1695–1697 (1985).
[49]T. Darden, D. York, and L. Pedersen, J. Chem. Phys. **98**, 10089–10092 (1993).
[50]U. Essmann, L. Perera, M. L. Berkowitz, T. Darden, H. Lee, and L. G. Pedersen, J. Chem. Phys. **103**, 8577–8597 (1995).
[51]R. J. Sadus, *Molecular Simulation of Fluids: Theory, Algorithms and Object-orientation* (Elsevier, Amsterdam, 1999).
[52]M. P. Allen and D. J. Tildesley, *Computer Simulation of Liquids* (Oxford University Press, New York, 1987).
[53]G. Raabe and R. J. Sadus, J. Chem. Phys. **137**, 104512 (2012).
[54]M. A. González and L. F. Abascal, J. Chem. Phys. **132**, 096101 (2010).
[55]G. J. Guo and Y. G. Zhang, Mol. Phys. **99**, 283 (2001).
[56]D. Alfe and M. Gillan, Phys. Rev. Lett. **81**, 5161 (1998).
[57]S. Plimpton, J. Comput. Phys. **117**, 1–19 (1995).
[58]C. Vega and E. de Miguel, J. Chem. Phys. **126**, 154707 (2007).
[59]P. J. In't Veld, A. E. Ismail, and G. S. Grest, J. Chem. Phys. **127**, 144711 (2007).
[60]J. K. Badenhoop and F. Weinhold, J. Chem. Phys. **107**, 5422–5432 (1997).
[61]See supplementary material at http://dx.doi.org/10.1063/1.4903928 for tables with numerical values of the vapor pressures, densities, viscosities, interfacial tensions, their corresponding statistical uncertainties, and figures with the Na^+–Cl^- pair correlation functions.
[62]Z. Mester and A. Z. Panagiotopoulos, "Mean ionic activity coefficients in aqueous NaCl solutions from molecular dynamics simulations," J. Chem. Phys. (submitted).
[63]S. L. Phillips, A. Igbene, J. A. Fair, H. Ozbek, and H. Tavana, *A Technical Databook for Geothermal Energy Utilization* (Lawrence Berkeley Laboratory, UC Berkeley, 1981) available at http://escholarship.org/uc/item/5wg167jq.
[64]A. A. Abramzon and R. D. Gauberk, Zh. Prek. Khim. **66**, 1428 (1993).